NANO LETTERS

Atomic Scale Structure Changes Induced by Charged Domain Walls in Ferroelectric Materials

Linze Li,[†] Peng Gao,[†] Christopher T. Nelson,[†] Jacob R. Jokisaari,[†] Yi Zhang,[†] Sung-Joo Kim,[†] Alexander Melville,[‡] Carolina Adamo,[‡] Darrell G. Schlom,[‡,§] and Xiaoqing Pan*,[†]

[†]Department of Materials Science and Engineering, University of Michigan, Ann Arbor, Michigan 48109, United States
[‡]Department of Materials Science and Engineering, Cornell University, Ithaca, New York 14853, United States
[§]Kavli Institute at Cornell for Nanoscale Science, Ithaca, New York 14853, United States

ABSTRACT: Charged domain walls (CDWs) are of significant scientific and technological importance as they have been shown to play a critical role in controlling the switching mechanism and electric, photoelectric, and piezoelectric properties of ferroelectric materials. The atomic scale structure and properties of CDWs, which are critical for understanding the emergent properties, have, however, been rarely explored. In this work, using a spherical-aberration-corrected transmission electron microscope with subangstrom resolution, we have found that the polarization bound charge of the CDW in rhombohedral-like $BiFeO_3$ thin films not only induces the formation of a tetragonal-like crystal structure at the CDW but also stabilizes unexpected nanosized domains with new polarization states and unconventional domain walls. These findings provide new insights on the effects of bound charge on ferroelectric domain structures and are critical for understanding the electrical switching in ferroelectric thin films as well as in memory devices.

KEYWORDS: Charged domain wall, bound charge, tetragonal-like bismuth ferrite, spherical-aberration-corrected transmission electron microscopy
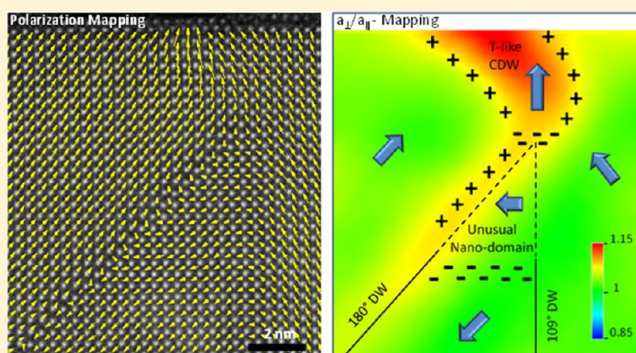
As the dimensions of individual elements in electronic devices continue to shrink, interfaces in strongly correlated systems have become more and more important. Engineering interfaces provides a powerful means to manipulate charge, spin, orbital, and lattice degrees of freedom in materials. Domain walls are homointerfaces in ferroic materials, and despite their study for more than 50 years they are attracting increasing attention due to the unique properties and novel functionalities they can possess with respect to the bulk material.[1−9] Compared to heterointerfaces, which separate different materials, domain walls can be easily manipulated by external magnetic, electric, or strain fields, allowing their useful properties to be actively modulated.

Domain walls in ferroelectric materials can carry net bound charge, resulting from a "head-to-head" or "tail-to-tail" polarization configuration, which is commonly observed in polarization switching processes.[10−15] The bound charge at such charged domain walls (CDWs) can gather compensating free charges, resulting in an insulator−metal transition at the CDWs.[13] The accumulation of oxygen vacancies at a CDW has been found to effectively lower the local energy bandgap and enhance the photocurrent.[14] On the other hand, the bound charge at a CDW can also affect the properties of the surrounding material by producing a depolarization field. Such a depolarizing field can lead to increased electromechanical

response and therefore improved piezoelectric properties.[16] It could also cause instability in the switching process and cause retention failure.[15]

To understand the underlying mechanisms of such emergent phenomena, it is crucial to study the effect of the bound charge at the CDWs on the structure and properties of ferroelectrics at the atomic scale. In this work we determine the atomic structure and ferroelectric polarization configurations of CDWs using spherical aberration (Cs) corrected transmission electron microscope (TEM) and quantitative atomic displacement and strain mapping techniques. We find in an epitaxial $BiFeO_3$ thin film with the rhombohedral-like (R-like) perovskite structure (Figure 1a left), the CDW possesses a tetragonal-like (T-like) crystal structure (Figure 1a, right) with a large c/a ratio (∼1.15), where the orientation of the ferroelectric polarization rotates from the ⟨111⟩ direction in the regular R-like domains to the c-axis at the T-like CDW. As a result, unusual nanosized domains with a pseudocubic perovskite structure but an in-plane oriented polarization are stabilized in the nearby regions.
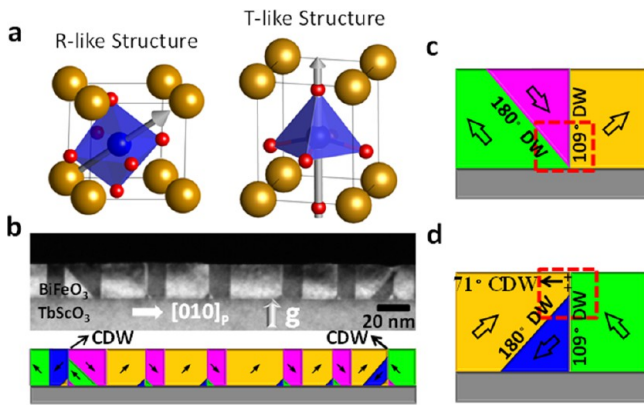
Figure 1. (a) Atomic models of the rhombohedral-like (R-like) and tetragonal-like (T-like) structures of $BiFeO_3$. (b) Cross-sectional dark-field TEM image showing the domain structure of a 20 nm thick $(001)_P$ $BiFeO_3$ film grown on a $(110)_O$ $TbScO_3$ substrate. A schematic of the corresponding domain configuration is shown below the TEM image. Schematic domain configurations of triangular 109°/180° domain wall junctions located (c) at the $BiFeO_3$/$TbScO_3$ interface without a CDW and (d) near the free surface with a CDW.

The $(001)_P$ oriented 20 and 5 nm thick $BiFeO_3$ films were grown on $(110)_O$ orthorhombic $TbScO_3$ substrates by the same molecular-beam epitaxy (MBE) method described in ref 17, with the $[100]_P \parallel [1\bar{1}0]_O$ and $[010]_P \parallel [001]_O$ directions (for simplicity, the subscripts P and O are used to represent pseudocubic and orthorhombic indices, respectively). Using Cs corrected scanning transmission electron microscopy (STEM), we employ high-angle annular dark field (HAADF) imaging (also known as "Z-contrast" imaging) performed at the TEAM 0.5 microscope with a point resolution of 0.5 Å to study the atomic-scale details of this system. The images were processed, following our previous work,[17] to allow accurate mapping of the lattice parameters and atomic displacement. To map the lattice parameters, data from the Bi sublattice was used since it has a stronger intensity and thus less noise. To map the displacement between the Fe and Bi atoms, we define a vector $\mathbf{D}_{FB}$, which is the atomic displacement in the image plane of the Fe cation from the center of the unit cell formed by its four Bi neighbors. In both the R-like and T-like structures in $BiFeO_3$, $\mathbf{D}_{FB}$ points toward the center of the negative oxygen charges and thus is opposite to the polarization vector in the image plane $\mathbf{P}_{plane}$.[17,18]

The domain structure of the 20 nm thick $BiFeO_3$ film is shown in a cross-sectional dark-field diffraction TEM image (Figure 1b). The domain configuration is depicted schematically below the TEM image, where the polarization vector orientations were confirmed by mapping $-\mathbf{D}_{FB}$ based on Z-contrast images. As it has been shown that only r_1/r_4 ferroelastic structures exist in such films[17,19] and that specific domain walls are constrained within specific planes,[20] it can be determined that the vertical boundaries are 109° domain walls and the inclined domain boundaries are 180° domain walls. Typically, the 180° domain walls appear paired with 109° ones to form triangular 109°/180° domain wall junctions, located either at the $BiFeO_3$/$TbScO_3$ interface (Figure 1c) or near the free surface (Figure 1d). Surprisingly, the latter junctions are usually located below the surface and thus create 71 °CDWs with "head-to-head" polarization arrangements.

The atomic scale structure and polarization configuration at the 109°/180° domain wall junctions were examined by ultrahigh resolution Z-contrast imaging. Figure 2a shows a Z-contrast image of domain walls terminating at the $BiFeO_3$/$TbScO_3$ interface. A color map in Figure 2b shows the direction distribution of $-\mathbf{D}_{FB}$, which is parallel to the $\mathbf{P}_{plane}$. Figure 2c shows the corresponding spatial distribution of the $-\mathbf{D}_{FB}$ vectors for the highlighted region in Figure 2b. Figure 2d shows the out-of-plane lattice parameter $(a_\perp)$/in-plane lattice
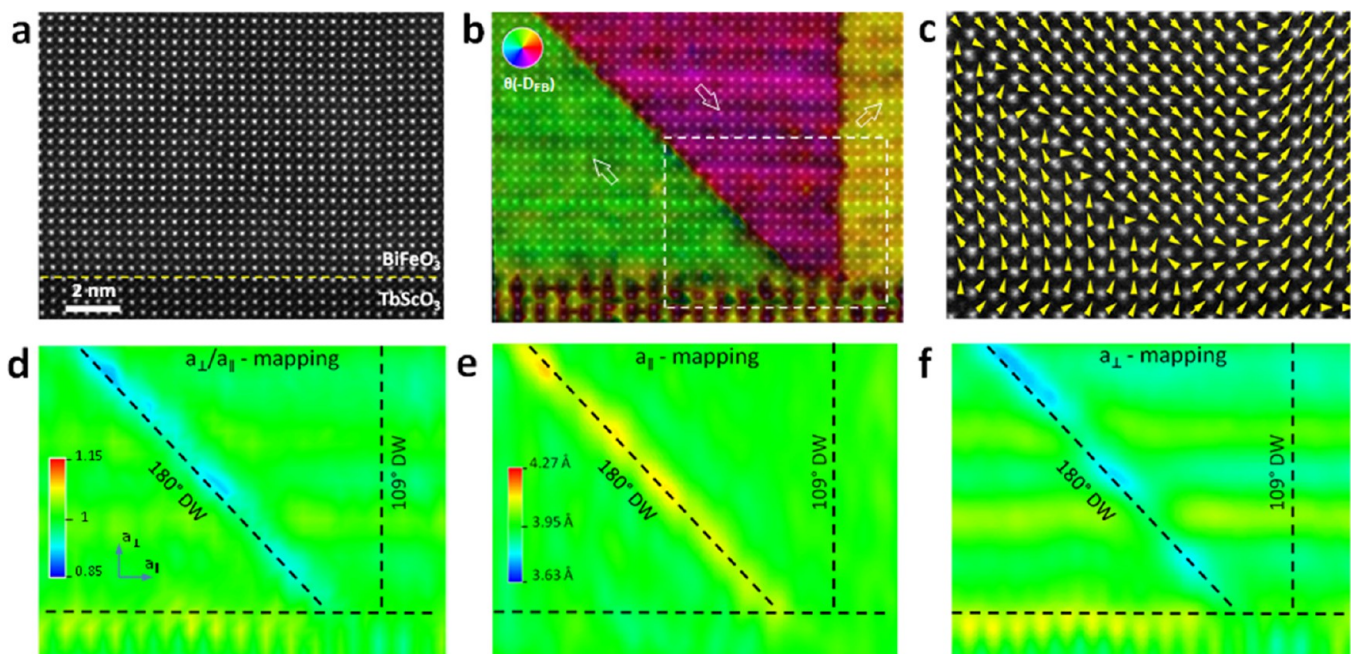
Figure 2. (a) Z-contrast STEM image of a triangular 109°/180° domain wall junction at the $BiFeO_3$/$TbScO_3$ interface without a CDW, similar to the highlighted region in Figure 1c, with the corresponding (b) color map of the direction of $-\mathbf{D}_{FB}$ and (c) the spatial distribution of the $-\mathbf{D}_{FB}$ vectors for the rectangular highlighted part in b, and color maps of (d) the $a_\perp/a_\parallel$ ratio, (e) the in-plane lattice parameter $a_\parallel$, and (f) the out-of-plane lattice parameter $a_\perp$.
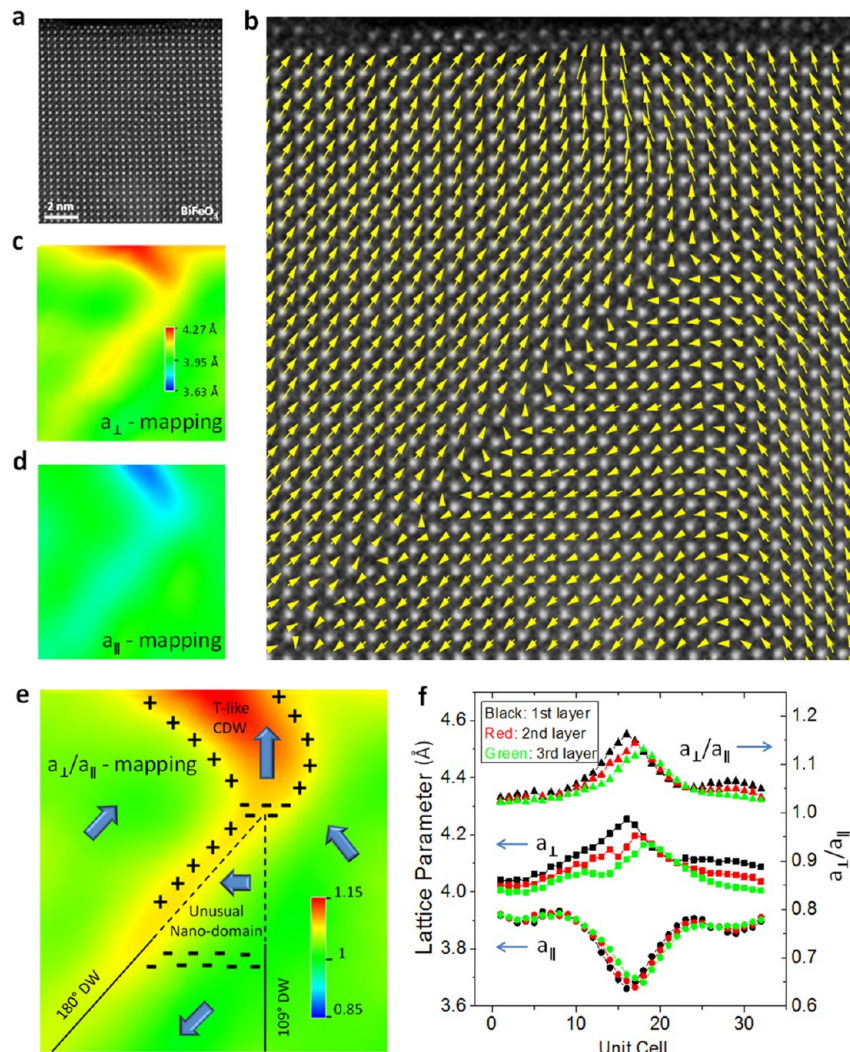
Figure 3. (a) Z-contrast STEM image of the triangular 109°/180° domain wall junction associated with a CDW near the free surface, similar to the highlighted region in Figure 1d, with the corresponding (b) spatial distribution of the $-D_{FB}$ vectors and color maps of (c) the out-of-plane lattice parameter $a_\perp$, (d) the in-plane lattice parameter $a_\parallel$, and (e) the $a_\perp/a_\parallel$ ratio. The polarization orientation and bound charge are indicated schematically in e, suggesting formation of a T-like CDW and an unusual nanodomain. (f) The $a_\perp$, $a_\parallel$, and $a_\perp/a_\parallel$ changes across the CDW in the first three lattice layers below the surface.

parameter $(a_\parallel)$ ratio $a_\perp/a_\parallel$ mapping of the Z-contrast image shown in Figure 2a, suggesting that the $a_\perp/a_\parallel$ ratio at the 180° domain walls is reduced compared with that of the bulk domain. This might be caused by the fact that domain walls in R-like $BiFeO_3$ tend to adopt an in-plane oriented polarization as an intermediate state.[21,22] In an inclined 180° domain wall, such polarization favors a lattice distortion with an increased in-plane lattice parameter and a reduced out-of-plane lattice parameter, as shown in Figure 2e and f, respectively. As the 109° domain wall is orientated vertically, however, the lattice distortion is forbidden by the clamping effect of the surrounding domains.

Figure 3a shows a Z-contrast image of a 109°/180° domain wall junction near the free surface of the same $BiFeO_3$ film. The spatial distribution of the $-D_{FB}$ vectors is shown in Figure 3b, revealing the formation of a CDW above the junction of the 180° and 109° domain walls. It is clearly shown that this polarization configuration does not result in a direct "head-to-head" boundary. In fact, the polarization rotates gradually from the $\langle 111 \rangle$ direction in the domains on both sides to the out-of-plane direction at the CDW. The crystal structure also changes

gradually across the CDW. Mapping of the lattice parameters (Figure 3c−e) shows that a decrease of the in-plane lattice parameter and an increase of the out-of-plane lattice parameter result in a high $a_\perp/a_\parallel$ ratio (~1.15) in the vicinity of the CDW. All of these results suggest the formation of a localized T-like structure at the CDW, while the surroundings remain in possession of R-like structure. Using the data from the top three lattice layers, the change of lattice parameters and $a_\perp/a_\parallel$ ratios across the CDW are plotted in Figure 3f, suggesting that the R to T then back to R structure transformation occurs over a distance of ~20 unit cells.

The formation of the T-like structure at the CDW can reduce the electrostatic energy by avoiding the formation of the direct "head-to-head" polarization configuration at the CDW. The coexistence of the T-like and R-like structures results in not only positive bound charge, but also compensating negative bound charge at the CDW, releasing some of the electrostatic energy, as shown schematically in Figure 3e. This is quite different from the well-known mixed R−T structures in strained $BiFeO_3$ thin films grown on $LaAlO_3$ substrates,[18,23−28] where the driving force is the highly
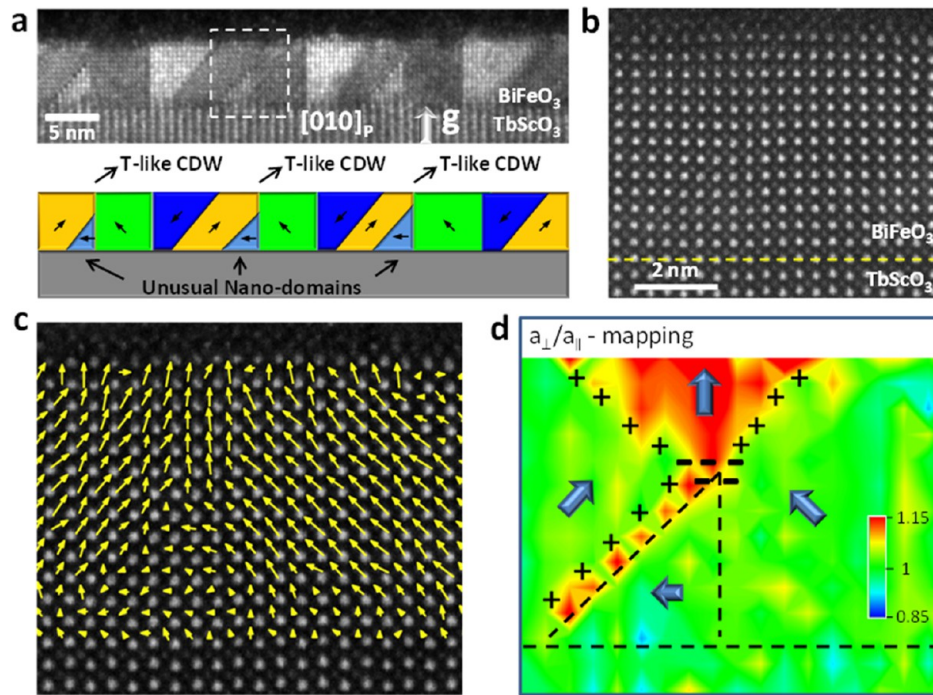
Figure 4. (a) Cross-sectional dark-field TEM image revealing the domain patterns of a 5 nm thick $(001)_P$ $BiFeO_3$ film grown on a $(110)_O$ $TbScO_3$ substrate. Arrays of T-like CDWs and unusual nanodomains are evident. (b) Z-contrast STEM image of the rectangular highlighted part in a, and the corresponding (c) spatial distribution of the $-\mathbf{D}_{FB}$ vectors and (d) color map of the $a_\perp/a_\parallel$ ratio. The polarization orientation and bound charge are indicated schematically in d, suggesting that a conductive CDW channel can form traversing the $BiFeO_3$ film.

compressive epitaxial strain. Due to the different formation mechanism, the R–T structure mixing observed here shows unique characteristics compared with that observed in the strained $BiFeO_3$ films grown on $LaAlO_3$. First, the R–T structure mixing in the $BiFeO_3/LaAlO_3$ system is limited to films thicker than 50 nm since it depends on relaxation of the epitaxial misfit strain. In contrast, in $BiFeO_3$ films on $TbScO_3$ substrates the dimension of the mixed R–T region is much finer, with the R and T domains as small as several nanometers in width. Second, unlike the strain driven mixed phase, where the in-plane lattice parameter of $BiFeO_3$ is constrained by the substrate lattice parameter and only changes slightly between the two phases (less than 3%), a significant decrease of the in-plane lattice parameter is observed in the T-like structure at the CDW, and the in-plane lattice parameters of the T-like structure at the CDW and the neighboring R-like phase differ by ∼8%.

The bound charge at the T-like CDWs also affects the polarization configuration in the region below the domain wall junction. As shown in Figure 3b and e, the tip region of the triangular domain below the CDW is found to possess an unexpected ferroelectric state, as its $a_\perp/a_\parallel$ ratio is close to 1.00, but its polarization is suppressed in magnitude and has rotated from the ⟨111⟩ direction to the in-plane direction. This avoids a direct "tail-to-tail" configuration at the triangular tip and thus releases some of the electrostatic energy. Due to the unique polarization state of this nanoregion, the rotation angle of polarization across the domain walls formed with the neighboring domains is no longer 180° or 109°, although they do return to those angles in the region far below the T-like CDW. The inclined wall (on the left side) of the triangular domain near the triangular tip becomes slightly charged itself, adopting an out-of-plane polarization as an intermediate state with respect to the two nearby domains (Figure 3b), and thus

has an increased $a_\perp/a_\parallel$ ratio (Figure 3e), which is exactly opposite to that of the uncharged 180° domain wall shown in Figure 2d. Moving down to the bottom interface, the polarization of the triangular domain returns to the ⟨111⟩ direction. As a result, the inclined 180° domain wall becomes neutral with a smaller $a_\perp/a_\parallel$ ratio.

For sufficiently thin films, an increased T/R ratio and CDWs traversing the full thickness of the film can be achieved. Arrays of charged and uncharged junctions of 180° and 109° domain walls were found in 5 nm thick $BiFeO_3$ films grown on $TbScO_3$ substrates (Figure 4a). The formation of the T-like CDW is also demonstrated in the higher magnification Z-contrast image (Figure 4b) and the corresponding spatial distribution of the $-\mathbf{D}_{FB}$ vectors and $a_\perp/a_\parallel$ ratio mappings in Figure 4c and d, respectively. As the triangular domain is much smaller in the 5 nm thick film, the whole triangular domain adopts a suppressed in-plane polarization, and the entire domain walls become unconventional, like those near the tip of the triangular domain in the 20 nm film, since the electrostatic driven force for these two regions is similar. Due to the effect of charges, the T-like CDWs and the unconventional CDWs of the unusual triangular domains can provide conducting channels running through the whole film in ferroelectric thin films.

Although the formation of a T-like structure at the CDW can provide self-compensating bound charges, the energy of such a CDW should still be higher than uncharged domain boundaries. The reason for the formation of the CDW near the free surface, rather at the $BiFeO_3/TbScO_3$ interface, is currently unclear. The energetic driving force for the formation of the CDW must be further considered. Whether the formation of a CDW is favorable depends on the minimization of the total domain wall energy:

$$E_{\text{total}} = E_{109}S_{109} + E_{180}S_{180} + E_{\text{CDW}}S_{\text{CDW}}$$
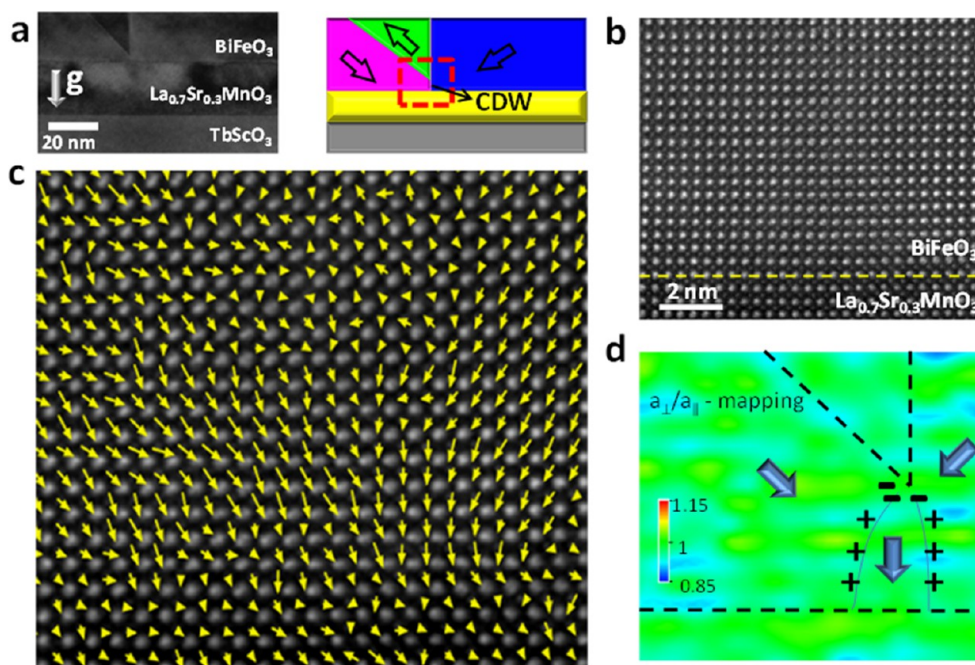
Figure 5. (a) Cross-sectional bright-field TEM images of domain patterns of a 20 nm thick $(001)_P$ $BiFeO_3$ film grown on a $(110)_O$ $TbScO_3$ substrate with a 20 nm thick $La_{0.7}Sr_{0.3}MnO_3$ bottom electrode. (b) Z-contrast STEM image of the rectangular highlighted part in a, with the corresponding (c) spatial distribution of the $-D_{FB}$ vectors, and (d) color map of the $a_\perp/a_\parallel$ ratio. The polarization orientation and bound charge are indicated schematically in d.

where E_{109}, E_{180}, E_{CDW}, S_{109}, S_{180}, and S_{CDW} are the energies per unit area and domain wall area of the 109° and 180° domain walls and the charged 71° domain wall (Figure 1d), respectively. When two 180° and 109° domain walls intersect with a junction below the free surface, adsorbed ions could provide free charge, compensating some of the bound charge at the CDW.[17,29] This results in a lowered E_{CDW}, comparable in energy to E_{109} and E_{180}.[30,31] The system will thus favor the formation of a CDW to decrease E_{total} by decreasing both S_{109} and S_{180}. When a CDW extends deeply in the $BiFeO_3$ film, however, E_{CDW} increases greatly as the free surface can no longer compensate the bound charge. As a result, CDWs are restricted to the near-surface region.

Since adsorbed surface charges are difficult to be seen directly in TEM, we also studied a $BiFeO_3$ film with a bottom electrode[17] to verify whether the free carriers in the electrode would be able to screen the bound charge of a CDW near the interface. The TEM image in Figure 5a shows the cross-sectional domain structure of a 20 nm thick $BiFeO_3$ film on an epitaxial 20 nm thick $La_{0.7}Sr_{0.3}MnO_3$ bottom electrode grown on a $(110)_O$ $TbScO_3$ substrate. In such a ferroelectric film, free charges are available at both the free surface due to adsorption and the bottom interface due to the existence of an electrode and may compensate some of the bound charge of a CDW. As a result, the CDWs are observed both near the bottom interface (Figure 5a) and near the surface (not shown). Consequently, we attribute the existence of the stable CDWs to charge compensation at the interfaces.

Close examination of CDWs formed near the bottom electrode show differences from those existing near the film surface. At the bottom electrode, substrate clamping restricts distortion of the crystal lattice of the $BiFeO_3$ film. A Z-contrast image of a CDW near the bottom interface is shown in Figure 5b, with the corresponding spatial distribution of the $-D_{FB}$ vectors and the $a_\perp/a_\parallel$ ratio mapping in Figure 5c and d,

respectively. The "head-to-head" polarization configuration below the triangular domain wall junction is evident, and a straight CDW forms. Although the polarization of the CDW rotates from the ⟨111⟩ direction to the out-of-plane direction to induce self-compensating bound charge, the $a_\perp/a_\parallel$ ratios of the CDW show no difference from the surrounding structures. Therefore, a new polarization state in the pseudocubic structure is stabilized at the CDW near the bottom electrode, in contrast to the T-like CDW structure formed near the free surface of the film.

In conclusion, utilizing quantitative TEM analysis of the atomic structure and the ferroelectric polarization configuration with the subangstrom precision, we have found stable charged domain walls (CDWs) in $BiFeO_3$ thin films. These CDWs possess crystal structures, ferroelectric polarization states, and properties different from the bulk film due to local charge compensation and polarization rotation. We have also found unconventional nanosized domains induced by the CDWs. These findings hold promise for novel applications of ferroelectric thin films in electronic and piezoelectric devices. This is because the nanodomains with unconventional polarization orientations as well as unique domain wall characteristics and the local properties of CDWs might be useful to control material properties at the nanoscale.

■ **AUTHOR INFORMATION**

Corresponding Author
*E-mail panx@umich.edu.

Notes
The authors declare no competing financial interest.

■ REFERENCES

(1) Seidel, J.; Martin, L. W.; He, Q.; Zhan, Q.; Chu, Y. H.; Rother, A.; Hawkridge, M. E.; Maksymovych, P.; Yu, P.; Gajek, M.; Balke, N.; Kalinin, S. V.; Gemming, S.; Wang, F.; Catalan, G.; Scott, J. F.; Spaldin, N. A.; Orenstein, J.; Ramesh, R. *Nat. Mater.* **2009**, *8* (3), 229–234.

(2) Seidel, J.; Maksymovych, P.; Batra, Y.; Katan, A.; Yang, S. Y.; He, Q.; Baddorf, A. P.; Kalinin, S. V.; Yang, C. H.; Yang, J. C.; Chu, Y. H.; Salje, E. K. H.; Wormeester, H.; Salmeron, M.; Ramesh, R. *Phys. Rev. Lett.* **2010**, *105* (19), 197603.

(3) Maksymovych, P.; Seidel, J.; Chu, Y. H.; Wu, P. P.; Baddorf, A. P.; Chen, L. Q.; Kalinin, S. V.; Ramesh, R. *Nano Lett.* **2011**, *11* (5), 1906–1912.

(4) Farokhipoor, S.; Noheda, B. *Phys. Rev. Lett.* **2011**, *107* (12), 127601.

(5) Guyonnet, J.; Gaponenko, I.; Gariglio, S.; Paruch, P. *Adv. Mater.* **2011**, *23* (45), 5377–5382.

(6) Choi, T.; Horibe, Y.; Yi, H. T.; Choi, Y. J.; Wu, W. D.; Cheong, S. W. *Nat. Mater.* **2010**, *9* (3), 253–258.

(7) Mostovoy, M. *Phys. Rev. Lett.* **2006**, *96* (6), 067601.

(8) Privratska, J.; Janovec, V. *Ferroelectrics* **1997**, *204* (1–4), 321–331.

(9) Privratska, J.; Janovec, V. *Ferroelectrics* **1999**, *222* (1–4), 23–32.

(10) Balke, N.; Gajek, M.; Tagantsev, A. K.; Martin, L. W.; Chu, Y. H.; Ramesh, R.; Kalinin, S. V. *Adv. Funct. Mater.* **2010**, *20* (20), 3466–3475.

(11) Nelson, C. T.; Gao, P.; Jokisaari, J. R.; Heikes, C.; Adamo, C.; Melville, A.; Baek, S. H.; Folkman, C. M.; Winchester, B.; Gu, Y. J.; Liu, Y. M.; Zhang, K.; Wang, E. G.; Li, J. Y.; Chen, L. Q.; Eom, C. B.; Schlom, D. G.; Pan, X. Q. *Science* **2011**, *334* (6058), 968–971.

(12) Gao, P.; Nelson, C. T.; Jokisaari, J. R.; Baek, S. H.; Bark, C. W.; Zhang, Y.; Wang, E. G.; Schlom, D. G.; Eom, C. B.; Pan, X. Q. *Nat. Commun.* **2011**, *2*, 591.

(13) Maksymovych, P.; Morozovska, A. N.; Yu, P.; Eliseev, E. A.; Chu, Y. H.; Ramesh, R.; Baddorf, A. P.; Kalinin, S. V. *Nano Lett.* **2012**, *12* (1), 209–213.

(14) Lee, W. M.; Sung, J. H.; Chu, K.; Moya, X.; Lee, D.; Kim, C. J.; Mathur, N. D.; Cheong, S. W.; Yang, C. H.; Jo, M. H. *Adv. Mater.* **2012**, *24* (10), Op49–Op53.

(15) Gao, P.; Nelson, C. T.; Jokisaari, J. R.; Zhang, Y.; Baek, S. H.; Bark, C. W.; Wang, E.; Liu, Y. M.; Li, J. Y.; Eom, C. B.; Pan, X. Q. *Adv. Mater.* **2012**, *24* (8), 1106–1110.

(16) Sluka, T.; Tagantsev, A. K.; Damjanovic, D.; Gureev, M.; Setter, N. *Nat. Commun.* **2012**, *3*, 748.

(17) Nelson, C. T.; Winchester, B.; Zhang, Y.; Kim, S. J.; Melville, A.; Adamo, C.; Folkman, C. M.; Baek, S. H.; Eom, C. B.; Schlom, D. G.; Chen, L. Q.; Pan, X. Q. *Nano Lett.* **2011**, *11* (2), 828–834.

(18) Zhang, J. X.; He, Q.; Trassin, M.; Luo, W.; Yi, D.; Rossell, M. D.; Yu, P.; You, L.; Wang, C. H.; Kuo, C. Y.; Heron, J. T.; Hu, Z.; Zeches, R. J.; Lin, H. J.; Tanaka, A.; Chen, C. T.; Tjeng, L. H.; Chu, Y. H.; Ramesh, R. *Phys. Rev. Lett.* **2011**, *107* (14), 147602.

(19) Folkman, C. M.; Baek, S. H.; Jang, H. W.; Eom, C. B.; Nelson, C. T.; Pan, X. Q.; Li, Y. L.; Chen, L. Q.; Kumar, A.; Gopalan, V.; Streiffer, S. K. *Appl. Phys. Lett.* **2009**, *94* (25), 251911.

(20) Streiffer, S. K.; Parker, C. B.; Romanov, A. E.; Lefevre, M. J.; Zhao, L.; Speck, J. S.; Pompe, W.; Foster, C. M.; Bai, G. R. *J. Appl. Phys.* **1998**, *83* (5), 2742–2753.

(21) Lubk, A.; Gemming, S.; Spaldin, N. A. *Phys. Rev. B* **2009**, *80* (10), 104110.

(22) Lubk, A.; Rossell, M. D.; Seidel, J.; He, Q.; Yang, S. Y.; Chu, Y. H.; Ramesh, R.; Hytch, M. J.; Snoeck, E. *Phys. Rev. Lett.* **2012**, *109* (4), 047601.

(23) Zeches, R. J.; Rossell, M. D.; Zhang, J. X.; Hatt, A. J.; He, Q.; Yang, C. H.; Kumar, A.; Wang, C. H.; Melville, A.; Adamo, C.; Sheng, G.; Chu, Y. H.; Ihlefeld, J. F.; Erni, R.; Ederer, C.; Gopalan, V.; Chen, L. Q.; Schlom, D. G.; Spaldin, N. A.; Martin, L. W.; Ramesh, R. *Science* **2009**, *326* (5955), 977–980.

(24) Mazumdar, D.; Shelke, V.; Iliev, M.; Jesse, S.; Kumar, A.; Kalinin, S. V.; Baddorf, A. P.; Gupta, A. *Nano Lett.* **2010**, *10* (7), 2555–2561.

(25) Damodaran, A. R.; Liang, C. W.; He, Q.; Peng, C. Y.; Chang, L.; Chu, Y. H.; Martin, L. W. *Adv. Mater.* **2011**, *23* (28), 3170–3175.

(26) Vasudevan, R. K.; Liu, Y. Y.; Li, J. Y.; Liang, W. I.; Kumar, A.; Jesse, S.; Chen, Y. C.; Chu, Y. H.; Nagarajan, V.; Kalinin, S. V. *Nano Lett.* **2011**, *11* (8), 3346–3354.

(27) Zhang, J. X.; Xiang, B.; He, Q.; Seidel, J.; Zeches, R. J.; Yu, P.; Yang, S. Y.; Wang, C. H.; Chu, Y. H.; Martin, L. W.; Minor, A. M.; Ramesh, R. *Nat. Nanotechnol.* **2011**, *6* (2), 97–101.

(28) Rossell, M. D.; Erni, R.; Prange, M. P.; Idrobo, J. C.; Luo, W.; Zeches, R. J.; Pantelides, S. T.; Ramesh, R. *Phys. Rev. Lett.* **2012**, *108* (4), 047601.

(29) Fong, D. D.; Kolpak, A. M.; Eastman, J. A.; Streiffer, S. K.; Fuoss, P. H.; Stephenson, G. B.; Thompson, C.; Kim, D. M.; Choi, K. J.; Eom, C. B.; Grinberg, I.; Rappe, A. M. *Phys. Rev. Lett.* **2006**, *96* (12), 127601.

(30) Gureev, M. Y.; Tagantsev, A. K.; Setter, N. *Phys. Rev. B* **2011**, *83* (18), 184104.

(31) Liu, Y. Y.; Liu, J. J.; Xie, S. H.; Li, J. Y. *Appl. Phys. Lett.* **2007**, *91* (17), 172910.